Experimental demonstration of second-order processes in photonic crystal microcavities at submilliwatt excitation powers

Murray W. McCutcheon, Jeff F. Young, and Georg W. Rieger
Department of Physics and Astronomy, University of British Columbia, Vancouver, Canada V6T 1Z1

Dan Dalacu, Simon Frédérick,* Philip J. Poole, and Robin L. Williams*
Institute for Microstructural Sciences, National Research Council, Ottawa, Canada K1A OR6
(Received 14 September 2007; revised manuscript received 12 November 2007; published 5 December 2007)

The far-field second-order radiation pattern from a wavelength-scale, InP-based photonic crystal microcavity that confines light in three dimensions is measured when excited on resonance by 300 μW of continuous-wave power from a laser diode. The measurements are accurately simulated using the finite-difference time-domain method, showing that both absorption and scattering play significant roles in determining the pattern of the radiation. The results show that the bulk second-order nonlinear susceptibility mediates the nonlinear process. In a separate set of experiments, a short-pulse laser is used to simultaneously populate two distinct modes of a similar microcavity. The detected second-order spectra show features due to the second harmonic generated by each mode, as well as the sum-frequency generation due to nonlinear intermode mixing. The key phenomena that determine the second-order response of these fundamentally small optical cavities are identified.

DOI: 10.1103/PhysRevB.76.245104 PACS number(s): 42.70.Qs, 42.65.Ky

I. INTRODUCTION

Few areas of photonics, indeed few areas of physics, have attracted as much attention over the past decade as photonic crystals (PhCs). While considerable theoretical work has identified several significant opportunities that PhCs offer in the context of enhanced nonlinear optical properties,[1–4] a remarkably small fraction of the published work has demonstrated that potential experimentally.

Perhaps the ultimate advantage offered by PhC engineering, in the nonlinear optics context, is the ability to localize light in wavelength-scale, three-dimensional (3D) microcavities, and keep it localized for many optical cycles. Cavities with quality (Q) factors over 10^6 and mode volumes on the order of one cubic wavelength in the host material have recently been reported.[5,6] The demonstrations of strong Rabi coupling of quantum dot excitonic transitions in more modest Q cavities[7,8] opened the path toward nonlinear processes at the cavity frequency in the quantum limit.[9] Cavities with much lower Q values have already been used to demonstrate classical hysteretic reflectivity behavior due to free-carrier generation at low (milliwatt) continuous-wave (cw) input powers.[10–13] It is perhaps not surprising that these types of nonlinear responses have so far received the most experimental attention, since they involve the same basic techniques commonly used to study the linear properties of the microcavities.

Measuring the second-order nonlinear optical response of PhC-based structures requires separate filtering and detection capabilities in addition to the resonant excitation setups used when only interested in the fundamental mode frequency range. This perhaps explains why detailed second-order experiments have been limited to relatively simple cavities that confine light in one dimension, using either Bragg stacks[14,15] or planar PhC membranes.[16–18]

This paper provides a comprehensive experimental demonstration of how multimode PhC microcavities that confine light in *three dimensions* enhance the *second-order* nonlinear response of the host material to the extent that harmonic radiation from intra- and intermode mixing in single cavities can be detected using submilliwatt excitation powers. After successfully simulating the nonintuitive polarization and far-field distribution properties of the harmonic radiation, we are able to show that despite the high surface-to-volume ratio in these PhC microcavities, the second-order material polarization in the microcavity is well described using the bulk second-order susceptibility of the InP host, and that the radiation it emits is strongly scattered out of the plane by the holes that define the photonic crystal around the cavity. These findings open other avenues for the dielectric engineering of integrated nonlinear photonic devices. In particular, they identify a way forward in designing wavelength-scale nonclassical light sources based on parametric down-conversion, another second-order nonlinear process intimately related to the sum-frequency generation process studied here.[19,20]

II. EXPERIMENTAL DETAILS

The second-order nonlinear properties of the PhC microcavities are studied by resonantly exciting the cavity modes with a free-space laser beam, either cw or pulsed, which is incident from a direction normal to the plane of the sample.[20,21] To acquire the second-order spectra, the scattered radiation from the microcavity is imaged through a spectrometer tuned to a spectral window around twice the mode frequency in order to detect evidence of a second-order nonlinear polarization being generated in the microcavity when the modes are excited. The transmission geometry is well suited for the second-order experiments, because it facilitates the use of two different microscope objectives to account for chromatic dispersion between the fundamental beam (ω) and the harmonic light ($\sim 2\omega$). A triple grating spectrometer and cooled charge-coupled device (CCD) array

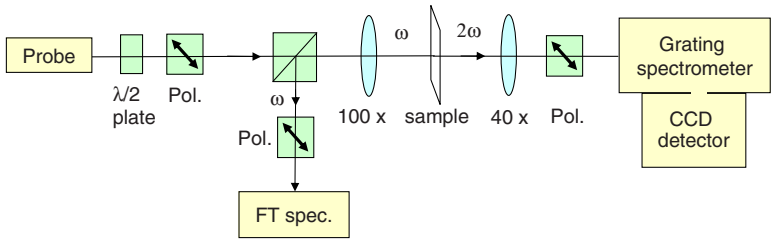

FIG. 1. (Color online) Second-order spectroscopy setup. The experiment is performed in transmission, allowing independent excitation and collection lens focal lengths. The second-order radiation can be spectrally resolved with a grating spectrometer, or imaged directly onto the CCD array. The resonant scattering spectrum is monitored in reflection with a Fourier transform (FT) spectrometer.

detector are used to measure the spectra of the second-order radiation. During the course of a second-order experiment, the reflected resonant scattering signal is monitored at the fundamental frequency to optimize and maintain the coupling to the desired mode. A schematic of the experimental setup is shown in Fig. 1.

For the cw experiments, the second-order radiation is *directly imaged* (no spectrometer) on the CCD array. This combines excellent sensitivity at the near infrared wavelengths of the harmonic radiation (~700–800 nm) with two-dimensional (2D) spatial resolution of the radiated light. Narrow band filters (10 nm full width at half maximum) centered at the second-order frequency of interest are required to filter out the fundamental beam and the residual second-harmonic generation (SHG) from the optical parametric oscillator (OPO). The CCD detector is placed directly behind the collection lens, which is positioned at its focal length behind the sample plane. In this configuration, a thin collection lens would precisely image the Fourier transform (i.e., the far fields) of the near-field distribution to a point a distance f behind the lens. Although the 40× microscope objective (a compound lens) used in collection is not a thin lens, empirically it was found to serve as a Fourier lens in this manner.

The InP membranes which host the PhC microcavities are 223 nm thick, and contain a dilute layer of InAs quantum dots at a density of 1–2 μm^{-2}. The quantum dots are only used as internal light sources to characterize the cavity modes, and are not implicated in any of the nonlinear processes discussed in this paper. Although all of these samples contain a similar layer of quantum dots, samples without quantum dots show a similar nonlinear response. The transmission experiments were facilitated by the fact that the samples consist of freestanding membranes mounted on a glass substrate. Details of the microcavity fabrication procedure are described in Ref. 22. The microcavities investigated in this work each consist of three missing holes in a 2D hexagonal photonic crystal, so-called L3 cavities. This was one of the first defect state geometries optimized to produce a relatively high-Q optical mode, with a mode volume on the order of one cubic wavelength.[23] While this is important for the present work, these cavities were also chosen because they actually support several relatively high-Q, polarized modes that lie both inside and outside the photonic band gap of the host hexagonal crystal. This allows us to demonstrate the full richness of the second-order interactions associated with these microcavities.

III. RESULTS AND DISCUSSION

The generic mode structure of an L3 microcavity in the frequency range of 180–220 THz is shown in Fig. 2, and the different modes studied here are highlighted. There are five peaks in the band gap corresponding to modes that are either x or y polarized, as indicated.[24] Just below the band edge, as determined by finite-difference time-domain (FDTD) simulations, there is another, *quasilocalized* (QL) mode, which has a much larger mode volume and/or area, and therefore, provides for an interesting comparison.[25]

A. Continuous-wave, single-mode excitation

We first consider an L3 cavity oriented such that the long axis of the cavity is aligned along the [110] electronic axis of the InP. As we will discuss below, in this cavity orientation, the TE-like fields of the confined radiation can efficiently drive second-order polarizations via the bulk nonlinear susceptibility. Samples with various orientations have been studied to help confirm that the bulk susceptibility gives the

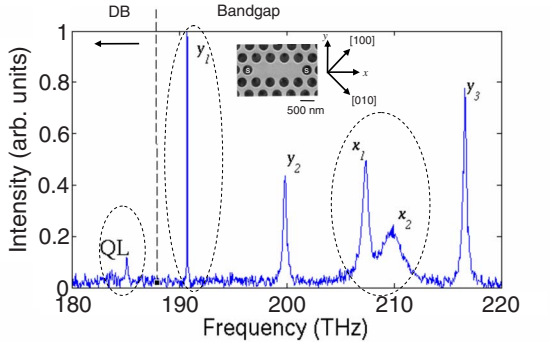

FIG. 2. (Color online) Photoluminescence (PL) spectrum from the InAs quantum dots distributed at a density of 1–2 μm^{-2} throughout the wetting layer in the middle of an L3 cavity (shown in the inset). There are three y-polarized and two x-polarized modes near the lower edge of the band gap, which extends from 188 to 260 THz, and one QL mode near the top of the dielectric band (DB). The relative orientation of the photonic axes (x,y) and InP crystal axes is shown. The circled modes are studied in different samples in this paper. The freestanding InP photonic crystals in this work are characterized by a lattice constant $a=510$ nm and a slab thickness $d=223$ nm. This PL spectrum is obtained from a sample with an air-hole radius $r=183$ nm and an outward side-hole shift $s=60$ nm (holes marked s) (Ref. 22).

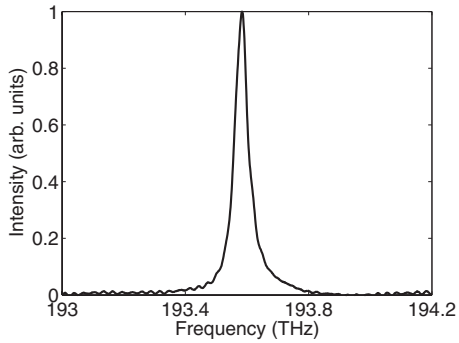

FIG. 3. cw resonant scattering spectrum of the fundamental mode (y_1) of an L3 microcavity.

dominant contribution to the second-order response, as shown below. A cw resonant scattering spectrum of the fundamental mode (y_1) of the cavity is plotted in Fig. 3. The mode is centered at 193.6 THz, and has a measured Q value of 3800, consistent with FDTD predictions. This relatively modest Q value reflects the nonoptimal side-hole shift of 30 nm (6% of the lattice spacing) in this particular sample. When the mode is excited on resonance by just 300 μW of cw laser diode radiation focused at normal incidence on the microcavity center and polarized along y, the SHG radiation (at 387.2 THz) collected in the far field normal to the slab has the pattern shown in Fig. 4(a). When a polarizer is placed in the collection path of the far-field radiation, it is found that the harmonic radiation at twice the cavity frequency is almost purely polarized along y. With the excitation frequency detuned by 1.4 THz to 192.2 THz, no clear radiation pattern could be detected in a 1 h integration on the liquid nitrogen cooled CCD camera, which puts a lower limit of a 1000:1 contrast in the SHG signal observed on and off resonance. In this normal incidence excitation geometry, we only expect to observe a fraction of the full Q^2 enhancement that could be realized if the cavity were resonantly excited by an overcoupled, single-channel waveguide.[20,26] Nevertheless, this simple experiment demonstrates the enormous local-field enhancement possible in such cavities.

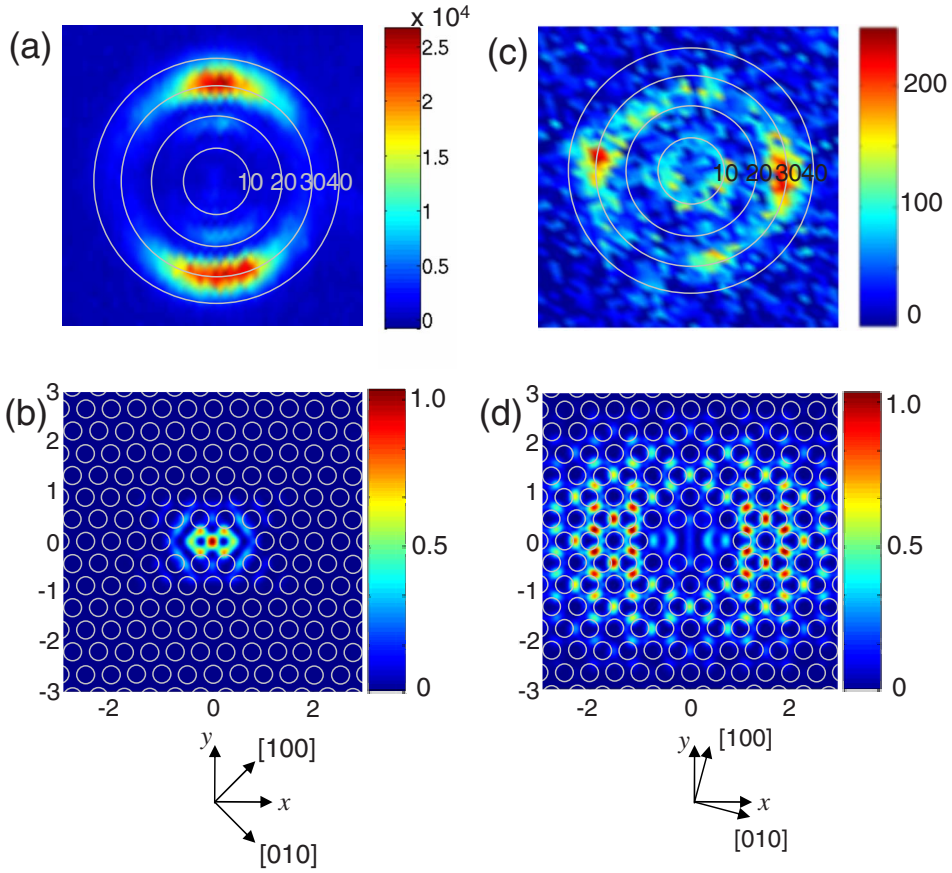

FIG. 4. (Color online) (a) CCD image of the second-order radiation pattern collected from the y_1 mode in Fig. 3 during a 2 h integration. The scale bar shows the total counts. The concentric rings show the solid angle of collection up to 40°, the limit of the NA=0.65 collection objective. The InP crystal axes are rotated by 45° with respect to the photonic axes (x,y). PhC parameters: hole radius r=189 nm, pitch a=510 nm, and shift of nearest neighbors s=30 nm. (b) Electric field intensity distribution of the y_1 mode in the middle plane of the slab as simulated by FDTD (dimensions are μm). (c) Second-order radiation pattern collected during a 15 min integration from a quasilocalized mode, which has the simulated $|E|^2$ distribution shown in (d). The scale bar in (c) shows the total counts. The InP crystal axes for the sample studied in (c) are rotated by 15° with respect to the cavity frame. PhC parameters: r=192 nm, a=510 nm, and s=15 nm. The intensity scales in (b) and (d) are arbitrary.

Figure 4(c) shows the far-field second-harmonic radiation pattern obtained when the same cw laser is used to excite one of the QL modes of a slightly different defect cavity oriented with its y axis at 15° to the [100] axis of the InP crystal. The QL mode lies 2 THz below the dielectric band edge, similar to the one evident in Fig. 2, and has a measured $Q \sim 3500$. It is insightful to compare the SHG radiated in the far field from these two modes, which have similar Q values but very different mode distributions, as shown in the simulations of Fig. 4. The fundamental cavity mode radiates polarized radiation almost exclusively at relatively high spatial frequencies, and preferentially in the y-z plane. The QL mode radiates almost unpolarized SHG radiation much more uniformly, both in angular and absolute spatial frequency domains. This is qualitatively consistent with the much more delocalized (in-plane) mode intensity distribution for the QL mode, which is mostly outside the cavity and in close proximity to the holes that comprise the background photonic crystal.

To put these observations on a more quantitative footing, we now compare the measured far-field SHG pattern from the fundamental y_1 mode with FDTD simulations. Figure 4(b) shows the 2D intensity distribution of the y_1 mode at the center of the InP membrane. All of the field components are in the plane of the membrane. That a mode with dominantly in-plane field components in a [001] oriented InP slab should radiate such a second-harmonic signal is not at all obvious. The bulk InP second-order susceptibility, which has only three nonzero components, $\chi^{(2)}_{ijk}(i \neq j \neq k)$, couples in-plane driving fields to out-of-plane z-oriented second-order polarizations, which will radiate dominantly in the plane. In the absence of the photonic crystal texturing, such radiation would be effectively guided in the plane of the slab due to the high refractive index contrast of the slab compared to the air cladding. Any radiation collected normal to the slab would be expected to be weak, isotropic, and unpolarized, contrary to the observations.

Although it is tempting to attribute these seemingly anomalous properties to the large surface-to-volume ratio of the microcavity, which breaks the bulk symmetry, it turns out that the pattern observed in the experiment can be simply reproduced by FDTD simulations that only include the bulk InP symmetry. Each of the seven main antinodes in the mode intensity profile of Fig. 4(b) has dominant field components oriented along either the [110] or [1$\bar{1}$0] directions of the InP crystal, and therefore, efficiently drives a z polarization, $P^{(2)}_z$, via the $\chi^{(2)}_{zjk}$ tensor component. This $P^{(2)}_z$ pattern, shown in Fig. 5(a), is modeled by a sum of discrete dipoles driven at the peak of the second-harmonic radiation spectrum, 387.2 THz, with amplitudes and phases (+ or −) scaled to match Fig. 5(a). A rigorous simulation in the undepleted pump approximation would involve taking $P^{(2)}_z$ from the linear simulations [Fig. 5(a)], sampling this on the FDTD mesh, and inserting a set of dipoles, one at each mesh point, to serve as the driving source. Given that the exact polarization distribution has a sharply peaked, discrete nature, a simplifying approximation is to concentrate the average dipole moment in the vicinity of each peak at a single point in space, and this procedure does effectively capture the experimental results.

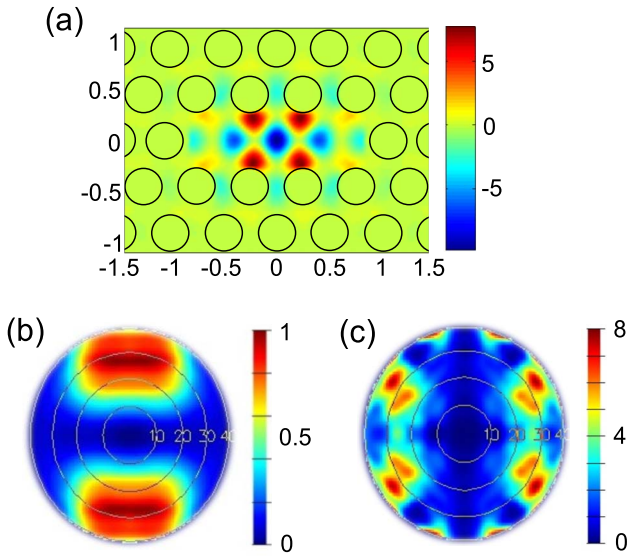

FIG. 5. (Color online) (a) z-oriented second-order polarization distribution for the y_1 mode simulated using FDTD (intensity scale is arbitrary). Far-field images of $|E|^2$ generated when the P_z distribution in (a) is modeled by a sum of discrete dipoles in an InP slab (b) with and (c) without absorption. The image in (b) well reproduces the experimental data of Fig. 4(a). The numeric values of the scale bars in (b) and (c) refer to the same absolute scale.

The near fields generated by this second-order polarization distribution are monitored just above the slab, and a near-field to far-field transformation is used to generate the far-field harmonic radiation patterns in Figs. 5(b) and 5(c). The image in Fig. 5(b) includes the effect of material absorption, which is significant (n=3.47, k=0.22) at the above-band-gap frequency of the second-harmonic radiation, whereas Fig. 5(c) accounts for just the real part (n=3.47, k=0), yielding a significantly different spatial pattern. Moreover, the pattern in Fig. 5(b) is almost purely polarized along y, whereas Fig. 5(c) has significant intensity in both polarizations. The good agreement of Fig. 5(b) with the experimental data of Fig. 4(a), in terms of spatial distribution and polarization, reveals the importance of material absorption and scattering from the boundaries of the rectangular-shaped microcavity in determining the nature of the far-field radiation. It also shows that the bulk $\chi^{(2)}$ tensor captures the main features of this second-order process inside the cavity.

B. Pulsed, multimode excitation

The L3 cavity allows us to further illustrate the second-order mixing of distinct, well-characterized, nondegenerate modes. Such interactions are fundamental to difference-frequency generation, which in these cavities could be tuned through the terahertz spectrum, and nondegenerate parametric down-conversion, which is relevant for the possible use of these cavities as entangled photon sources.[19,20] Here, we characterize the sum-frequency mixing of the two x-polarized modes, labeled x_1 and x_2 in Fig. 2, by using a broadband source to simultaneously populate both modes. Figure 6 shows the spectrum of the radiation emitted from a

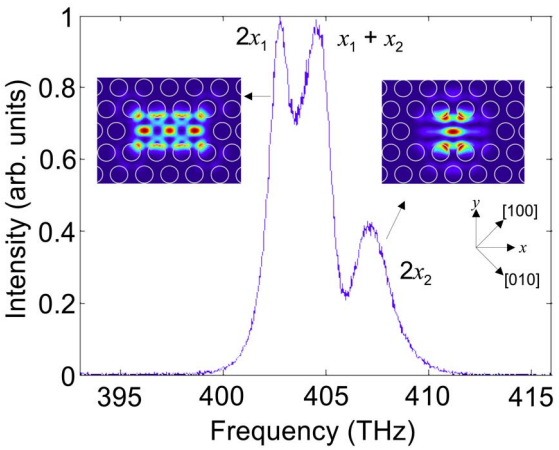

FIG. 6. (Color online) Second-order radiation spectrum acquired when a train of 130 fs laser pulses is used to excite the x-dipole modes (Ref. 27) in a PhC microcavity with $r=165$ nm and $s=60$ nm. The insets show $|E|^2$ in the middle plane of the slab for each mode.

microcavity sample in the vicinity of twice the energy of the x-polarized modes when the cw laser diode excitation is replaced with an 80 MHz train of 130 fs pulses obtained from the signal beam output of an OPO. The spectrum of the 130 fs pulses, which deliver an average power of 1 mW at normal incidence on the microcavity, is broad enough to simultaneously excite both x modes,[27] and the harmonic spectrum clearly shows evidence of both the SHG from the nonlinear self-interaction of each mode and a third peak that is due to sum-frequency generation from the second-order interaction of the two distinct modes. We have observed this sum-frequency generation from simultaneously populated modes in single missing hole and L3 cavities, involving both localized and QL states. In all our experiments, the second-order peaks are compared to linear resonant scattering spectra to show an exact correspondence of the various features.[21] The polarization properties of the sum-frequency radiation depend on the orientation of the electronic and photonic crystal axes, but its maximum strength is typically similar to the SHG from each mode individually. Although the two modes were simultaneously excited by a single source in this example, the process could be used to optically monitor joint occupancy if independent channels were used to store photons in the cavity as part of a multichannel optical processor.

A high conversion efficiency was not the goal of this work, and the ratio of the collected harmonic radiation power to the average excitation power is $\sim 10^{-13}$ for the data shown in Fig. 4(a). This reflects the nonoptimized excitation and collection geometries, and the fact that the second-harmonic frequency in this demonstration is actually above the band gap of the host InP, which therefore absorbs it strongly. There may be an advantage to having a second-harmonic signal above the band gap, for example, in an optoelectronic device designed to detect the generated free carriers. However, if a higher conversion efficiency is desired, the structure could be optimized by coupling light to the microcavity via a one-dimensional waveguide channel, engineering the second-order frequencies to be below the band gap, and, more ambitiously, designing a doubly resonant microcavity for which both the fundamental and second-harmonic fields are locally enhanced.[11,28,29]

IV. CONCLUSIONS

In summary, 3D-localized defect states in InP-membrane-based 2D photonic crystals generate easily detected second-order radiation when excited by less than 1 mW of average optical power, either cw or as an 80 MHz train of 130 fs pulses. By favorably comparing to FDTD simulations the measured far-field pattern of the polarized harmonic radiation from the fundamental high-Q mode of an L3 cavity, we verified that it is due to a second-order polarization oriented normal to the surface of the membrane scattering strongly from the nearest holes that define the cavity. Thus, the bulk InP second-order susceptibility, rather than symmetry-breaking contributions near the holes, can be used to model second-order processes involving cavity modes in this system. When the harmonic radiation is above the electronic band gap energy of the InP, the absorption has a considerable effect on the radiation pattern. When more than one mode is excited, the sum-frequency mixing of the distinct modes is comparable in intensity to the harmonic from each mode, and their relative polarization properties can be manipulated by varying the relative orientation of electronic and photonic crystal axes. Observation of second-order mixing of distinct cavity modes suggests further studies of related difference-frequency and nondegenerate parametric down-conversion processes. By working with differently oriented InP wafers, and adjusting the parameters so that the harmonic radiation is below the electronic band gap, a number of opportunities are available to make use of these second-order properties in fully integrated waveguide/cavity structures where both the fundamental and harmonic frequencies are resonant with localized modes.

ACKNOWLEDGMENTS

The authors wish to acknowledge the financial support of the Natural Sciences and Engineering Research Council of Canada, the Canadian Institute for Advanced Research, the Canadian Foundation for Innovation, the Canadian Institute for Photonic Innovations, and the technical assistance of Lumerical Solutions Inc.

*Also at Department of Physics, University of Ottawa, Ottawa, Canada K1N 6N5.
[1] K. Sakoda and K. Ohtaka, Phys. Rev. B **54**, 5742 (1996).
[2] J. Vuckovic, M. Loncar, H. Mabuchi, and A. Scherer, Phys. Rev. E **65**, 016608 (2001).
[3] M. Soljačić and J. D. Joannopoulos, Nat. Mater. **3**, 211 (2004).
[4] A. R. Cowan and J. F. Young, Semicond. Sci. Technol. **20**, R41 (2005).
[5] T. Tanabe, M. Notomi, E. Kuramochi, A. Shinya, and H. Taniyama, Inst. Phys. Conf. Ser. **1**, 49 (2007).
[6] B. S. Song, S. Noda, T. Asano, and Y. Akahane, Nat. Mater. **4**, 207 (2005).
[7] J. P. Reithmaier, G. Sek, A. Loffler, C. Hofmann, S. Kuhn, S. Reitzenstein, L. V. Keldysh, V. D. Kulakovskii, T. L. Reinecke, and A. Forchel, Nature (London) **432**, 197 (2004).
[8] T. Yoshie, A. Scherer, J. Hendrickson, G. Khitrova, H. M. Gibbs, G. Rupper, C. Ell, O. B. Shchekin, and D. G. Deppe, Nature (London) **432**, 200 (2004).
[9] K. Hennessy, A. Badolato, M. Winger, D. Gerace, M. Atature, S. Gulde, S. Falt, E. L. Hu, and A. Imamoglu, Nature (London) **445**, 896 (2007).
[10] M. Soljačić, M. Ibanescu, S. G. Johnson, Y. Fink, and J. D. Joannopoulos, Phys. Rev. E **66**, 055601(R) (2002).
[11] A. R. Cowan and J. F. Young, Phys. Rev. B **65**, 085106 (2002).
[12] P. E. Barclay, K. Srinivasan, and O. Painter, Opt. Express **13**, 801 (2005).
[13] M. Notomi, A. Shinya, S. Mitsugi, G. Kira, E. Kuramochi, and T. Tanabe, Opt. Express **13**, 2678 (2005).
[14] T. V. Dolgova, A. I. Maidykovski, M. G. Martemyanov, A. A. Fedyanin, O. A. Aktsipetrov, G. Marowsky, V. A. Yakovlev, and G. Mattei, Appl. Phys. Lett. **81**, 2725 (2002).
[15] J. Trull, R. Vilaseca, J. Martorell, and R. Corbalan, Opt. Lett. **20**, 1746 (1995).
[16] J. P. Mondia, H. M. van Driel, W. Jiang, A. R. Cowan, and J. F. Young, Opt. Lett. **28**, 2500 (2003).
[17] A. M. Malvezzi, G. Vecchi, M. Patrini, G. Guizzetti, L. C. Andreani, F. Romanato, L. Businaro, E. Di Fabrizio, A. Passaseo, and M. De Vittorio, Phys. Rev. B **68**, 161306(R) (2003).
[18] J. Torres *et al.*, Phys. Rev. B **69**, 085105 (2004).
[19] D. Bouwmeester, J. W. Pan, K. Mattle, M. Eibl, H. Weinfurter, and A. Zeilinger, Nature (London) **390**, 575 (1997).
[20] M. G. Banaee, A. G. Pattantyus-Abraham, M. W. McCutcheon, G. W. Rieger, and J. F. Young, Appl. Phys. Lett. **90**, 193106 (2007).
[21] M. W. McCutcheon, G. W. Rieger, I. W. Cheung, J. F. Young, D. Dalacu, S. Frédérick, P. J. Poole, G. C. Aers, and R. L. Williams, Appl. Phys. Lett. **87**, 221110 (2005).
[22] D. Dalacu, S. Frédérick, A. Bogdanov, P. J. Poole, G. C. Aers, R. L. Williams, M. W. McCutcheon, and J. F. Young, J. Appl. Phys. **98**, 023101 (2005).
[23] Y. Akahane, T. Asano, B. S. Song, and S. Noda, Nature (London) **425**, 944 (2003).
[24] A. R. A. Chalcraft *et al.*, Appl. Phys. Lett. **90**, 241117 (2007).
[25] F. Bassani, G. Iadonisi, and B. Preziosi, Rep. Prog. Phys. **37**, 1099 (1974).
[26] P. E. Barclay, K. Srinivasan, M. Borselli, and O. Painter, Opt. Lett. **29**, 697 (2004).
[27] The higher energy x-dipole mode has a degenerate partner mode, but it has symmetric reflection symmetry about both x and y axes, and is therefore not excited in this geometry.
[28] M. Liscidini and L. C. Andreani, Phys. Rev. E **73**, 016613 (2006).
[29] L. C. Andreani and D. Gerace, Phys. Rev. B **73**, 235114 (2006).